

Ultrathin CdSe in Plasmonic Nanogaps for Enhanced Photocatalytic Water Splitting

Daniel O. Sigle,[†] Liwu Zhang,^{*,†,‡} Sandrine Ithurria,[§] Benoit Dubertret,[§] and Jeremy J. Baumberg^{*,†}

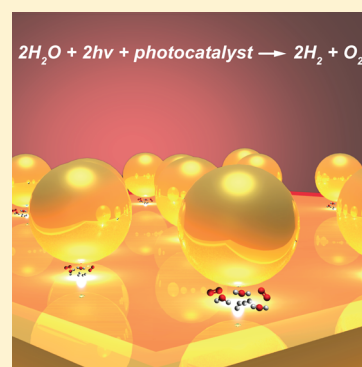
[†]NanoPhotonics Centre, Cavendish Laboratory, University of Cambridge, Cambridge CB3 0HE, United Kingdom

[‡]Department of Environmental Science and Engineering, Fudan University, Shanghai 200433, China

[§]LPEM, ESPCI-ParisTech, PSL Research University, CNRS, Sorbonnes Université, UPMC Paris VI, 10 rue Vauquelin, 75005 Paris, France

S Supporting Information

ABSTRACT: Enhanced plasmonic fields are a promising way to increase the efficiency of photocatalytic water splitting. The availability of atomically thin materials opens up completely new opportunities. We report photocatalytic water splitting on ultrathin CdSe nanoplatelets placed in plasmonic nanogaps formed by a flat gold surface and a gold nanoparticle. The extreme field intensity created in these gaps increases the electron–hole pair production in the CdSe nanoplatelets and enhances the plasmon-mediated interfacial electron transfer. Compared to individual nanoparticles commonly used to enhance photocatalytic processes, gap-plasmons produce several orders of magnitude higher field enhancement, strongly localized inside the semiconductor sheet thus utilizing the entire photocatalyst efficiently.



Hydrogen is a highly promising energy carrier due to its entirely neutral combustion process, with water as the only exhaust product. The major drawback for large-scale employment of hydrogen-fueled devices is a lack of efficient production. Various semiconductors have proven to enable photocatalytic water splitting into hydrogen and oxygen.^{1–3} Although existing technologies are generally complicated and of low efficiency, it has been demonstrated that the strongly enhanced electric field created by plasmonic nanostructures can lead to increased electron–hole pair (e–h-pair) production in nearby semiconductor crystals, which facilitates hydrogen production using solar energy.^{4–11} The availability of metallic nanoparticles of widely different shapes and sizes allows specific matching of the plasmonic resonance conditions to the semiconductor absorption bands and, therefore, optimizing the e–h-pair production.^{12,13}

One bottleneck commonly identified for photocatalytic water splitting is the limited charge carrier diffusion length in the semiconductor, typically below 20 nm.¹⁴ E–h-pairs created deeper in the bulk material cannot reach the surface and consequently do not contribute to the water splitting. Thin layers of semiconductor are therefore favorable to increase the yield for hydrogen production, but the efficiency in such thin slabs is usually limited by the low optical absorption cross-section.

Due to the strong localization of the optical field near plasmonic nanoparticles, the light intensity is channelled to the surface layers of the photocatalyst. However, compared to plasmons occurring in the vicinity of individual nanoparticles, up to 100-fold higher electric field enhancements are sustained

in gaps of only few nanometers between two nanoparticles or a nanoparticle spaced above a flat metallic surface.^{15,16} Gap plasmons in the nanoparticle-on-mirror (NPoM) geometry exhibit extremely localized electrical fields across the material inside the nanogap (Figure 1a). Although the plasmonic enhancement of individual nanoparticles for solar water splitting has been widely studied,^{17–19} no previous reports have focused on the enhanced photocatalysis generated in plasmonic nanogaps by using the much higher field intensities available.

The emergence of materials with single unit cell thickness such as graphene, MoS₂, or boron nitride are becoming ideal candidates for placement in such plasmonic nanogaps because the nanometer-spacing provided enables plasmonic coupling across the active material. This construct enables a variety of interesting phenomena such as their ultrasensitive interrogation via surface-enhanced Raman scattering.²⁰

In this paper, plasmon-enhanced photocatalytic water splitting from cadmium selenide (CdSe) nanoplatelets with a thickness of only 5 atomic layers or 1.7 nm²¹ is demonstrated (Figure 1b,c). The nanoplatelets are sandwiched between a flat gold surface and gold nanoparticles (AuNP). Illumination with broadband light excites strongly localized gap plasmons across the platelets. The occurrence of strongly coupled gap plasmons between AuNP and Au surface can be verified by a color change

Received: February 9, 2015

Accepted: March 9, 2015

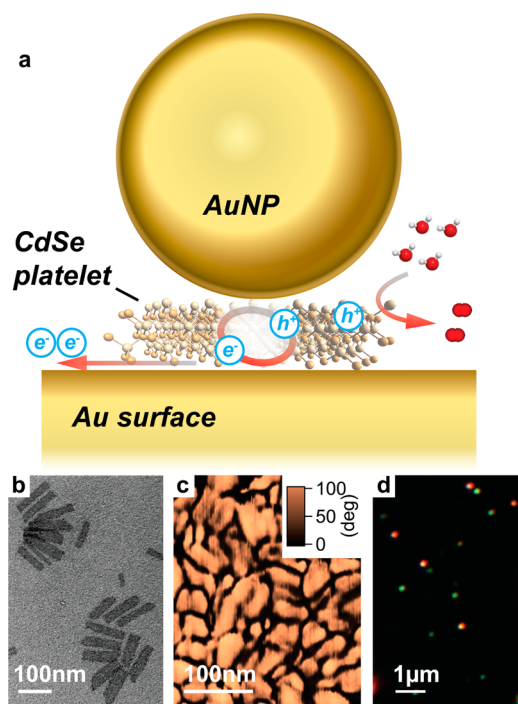


Figure 1. (a) AuNPs on gold film with atomically thin CdSe sandwiched between them. Charge oscillations in AuNPs induce image charges in the metallic surface and enable plasmonic coupling. (b) TEM of nanoplatforms. (c) AFM of nanoplatform monolayer on Au surface (phase image). (d) Dark Field scattering of sample surface with AuNPs spaced from the surface by nanoplatform layer.

of the dark-field scattering from green (indicating the plasmon resonance of uncoupled AuNPs) to red (coupled AuNPs), as shown in Figure 1d. The exact spectral response is highly sensitive to the specific morphology of each NPoM construct. With this configuration, the coupled plasmons completely penetrate the photocatalytic material as opposed to previous routes, in which only the surface layers benefit from increased e–h-pair generation. Further, the usual problem of charge recombination inside the catalyst is highly suppressed, as the carrier diffusion length greatly exceeds the thickness of the semiconductor.

Gold surfaces were coated with a single layer of CdSe platelets before adding 100 nm AuNP (see Methods). The surface coverage of CdSe is $\sim 70\%$ as verified with AFM (Figure 1c). For the photochemical water splitting experiments, the sample was studied both in the dark and under illumination of 200 mW cm^{-2} from a xenon light source.

A conventional three electrode configuration was used with the CdSe platelets in the NPoM geometry as the photoanode (working electrode), Pt wire (counter electrode), and Ag/AgCl as a reference electrode. Linear voltammetry sweeps (recorded at a scan rate of 10 mV/s) on the CdSe platelets in the NPoM geometry show a photocurrent increase with applied positive potential under illumination, whereas the currents are negligible in the dark. For comparison, experiments were carried out on AuNPs on a gold substrate in the absence of CdSe nanoplatforms, where negligible photocurrent is observed. The photocurrent measured on the CdSe platelets in the NPoM configuration was observed to be enhanced by approximately five times as compared with the CdSe platelets on the Au substrate without AuNPs on top (Figure 2a). This is a result from increased water oxidation within the plasmonic hotspots

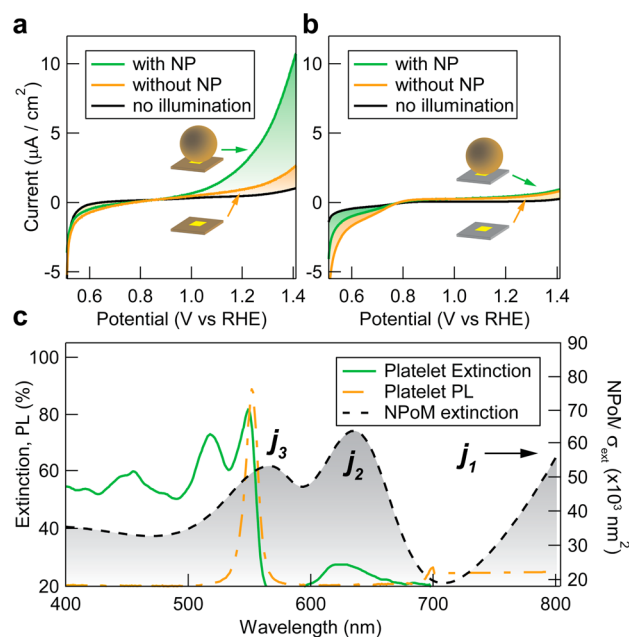


Figure 2. (a) Photocurrent from the CdSe platelets on gold surface in NPoM geometry (green), without AuNPs (orange), and without illumination (black). (b) Photocurrent from CdSe platelets on FTO surface, with (green) and without (orange) AuNPs. (c) Extinction and luminescence spectra of colloidal CdSe platelets and simulated NPoM extinction. The NPoM setup exhibits three plasmonic resonances (j_1 , j_2 , j_3), whereas j_3 overlaps with the electron/heavy-hole transition.

between AuNP and Au surface. Control experiments were conducted with the CdSe nanoplatforms placed on a fluorine-doped tin oxide (FTO) surface instead of the gold. FTO does not sustain plasmonic enhancements near the CdSe absorption bands. In this case the absence of gap plasmons does not generate a noticeable photocurrent enhancement as compared to the case without AuNPs (Figure 2b). Boundary-element (BEM) simulations show that the field intensity generated from individual (uncoupled) nanoparticles is more than 3 orders of magnitude weaker than the gap plasmons at the platelet absorption edge (Figure 3a) and not sufficient to generate a noticeable photocurrent increase. Given the sparse NP surface

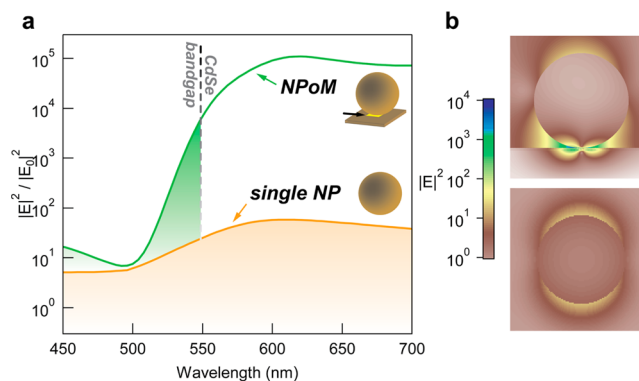


Figure 3. (a) BEM simulation of intensity enhancement $|E|^2/|E_0|^2$ in the nanogap and in the vicinity of a single nanoparticle. Dashed line marks the platelet optical bandgap transition. (b) Field enhancement at the optical bandgap of the CdSe platelets ($\lambda = 548 \text{ nm}$) in the NPoM-nanogap (top) and for an isolated AuNP (bottom) for comparison.

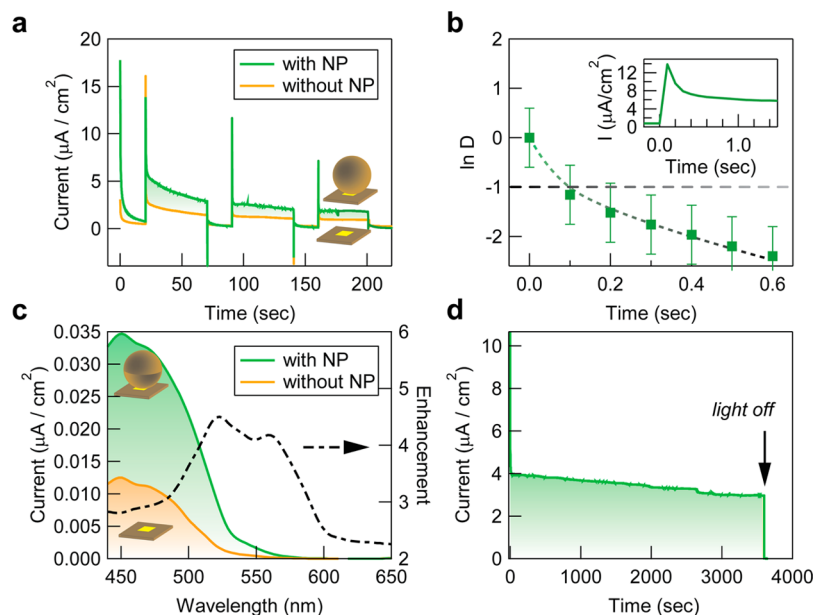


Figure 4. (a) Photocurrent transients at fixed potential of 0.5 V vs Ag/AgCl for chopped illumination with and without nanoparticles. (b) Transient decay time with NPs. Inset shows photocurrent spike after switching on the light (magnified from (a)). (c) Action spectra of the CdSe platelets on gold surface in NPoM (green) and without NPoM geometry (orange). The dotted curve shows the enhancement factor of the action spectrum for CdSe platelets sandwiched in NPoM. (d) Stability test of CdSe platelets in NPoM at 0.5 V vs Ag/AgCl.

coverage in these experiments, it is emphasized that the enhanced fields cover only a small fraction of the sample surface. Taking into account an AuNP density of $\sim 5 \times 10^5$ particles/mm² and using the hot spot width of ~ 20 nm obtained from the BEM simulations (Figure 3b), we estimate that the photocurrent locally generated inside the nanogaps is enhanced by roughly $\times 10^4$ over the bare platelet coated gold surface in the absence of AuNPs (calculation see Supporting Information). This indicates a figure for the theoretically possible enhancement in a plasmonic field, but is not easily scalable as the hot spots are confined to minuscule regions on a plasmonic device.

The origin of the strong plasmonic enhancement in the nanogap is explored with boundary element (BEM) simulations. Plasmonic coupling between nanoparticle and surface leads to three predominant modes as a result of particle–surface coupling, denoted as j_1 , j_2 , and j_3 (Figure 2c). These three modes are the fundamental solution (j_1) and higher orders of a nanoscale metal–insulator–metal waveguide formed by the nanoparticle and the surface.²² Although the fundamental mode (j_1) is located further in the infrared, j_2 and j_3 are close to the CdSe absorption bands. Mode j_3 overlaps with the electron/heavy-hole transition of the nanoplatelets at 550 nm and, hence, provides the major contribution to the amplified creation of e–h-pairs. The field enhancements produced in this nanometer-sized gap are strongly wavelength dependent. At the CdSe absorption edge, the field is enhanced by $|E|^2 \sim 10^4$ and is about 3 orders of magnitude higher than around an isolated nanoparticle (Figure 3).

The noticeable photocurrent increase in the NPoM configuration but negligible enhancement on the FTO surface suggests that the enhanced water splitting is mainly a result of the strongly localized gap plasmons across the CdSe sheets in the plasmonic nanogap rather than a single particle plasmon. Further, plasmon-mediated electron transfer from AuNPs, which has been extensively studied in recent years,^{14,17} can contribute to the observed photocurrent enhancement because

interfacial electron transfer from AuNP to the conduction band of CdSe is facilitated through the gap plasmon. The low photocurrent observed from AuNP-modified CdSe platelets on the FTO substrate indicates that the enhancement in Figure 2a is not caused by photocatalytic effects or any water oxidation catalytic effects of the AuNPs. It also suggests that catalytic properties of the Au substrate have no effect because the photocurrent is low in the case of CdSe-platelet-coated Au surfaces without AuNPs (Figure 2a).

To qualitatively understand the charge generation and recombination behavior in such thin catalytic films, the transient photocurrent decay was investigated (Figure 4). Here, the potential was kept constant at 0.5 V and chopped illumination was applied while recording the photocurrent as a function of time. When the light is switched on, a photocurrent spike occurs due to the sudden generation of charge carriers, which quickly recombine as seen from the rapid photocurrent decay (Figure 4a). The time scale of this transient decay can be determined by a logarithmic plot of parameter D , given by²³

$$D(t) = [I(t) - I_s] / [I_m - I_s]$$

where I_m is the spike photocurrent, I_s is the steady state photocurrent, and $I(t)$ is the photocurrent at time t (Figure 4b). The transient decay time is defined as the time at which $\ln D = -1$.

The transient decay time (Figure 4b) is < 100 ms for both samples with and without NPs. This photocurrent decay rate is determined by the degree to which the charge generation process is dominated by recombination. The steady-state current (I_s) is achieved when the recombination and charge generation reach equilibrium.^{24,25} In bulk semiconductors, the charge recombination rate is reduced in the presence of plasmonic fields^{26,27} as the field (and hence e–h-pair production) is channelled to the semiconductor surface whereas the charge recombination takes place in the bulk material. In these experiments, the plasmonic fields do not significantly affect the transient time as in the case of these

ultrathin semiconductor slabs the plasmon completely interpenetrates the material and the carrier diffusion length exceeds the thickness of the active media. Hence, in both cases—with and without nanoparticles—the charge carrier generation is homogeneous within the cross section of the CdSe slab and an increased carrier lifetime in the presence of nanoparticles is not observed. It is notable that the access of H₂O into and O₂ out of the plasmonic hot spot is thus not restricted by this nanogeometry, likely because the molecules are well coupled into the bulk solution.

Action spectra of the CdSe platelets in Au NPoM (green) and outside this NPoM geometry were also taken to investigate the spectral response of the photocurrent enhancement in the plasmonic nanogap (Figure 4c). The CdSe shows a higher photocurrent response than the CdSe outside this NPoM configuration over the entire investigated spectral range from 440 to 580 nm. The enhancement depends on the wavelength and peaks at $\times 4$ – 5 between 500 and 580 nm, but drops to $\times 2$ – 3 at shorter wavelengths where the plasmonic field enhancement decays. At wavelengths >600 nm, the photocurrent vanishes as the photon energy is lower than required to produce excitons in the 550 nm CdSe bandgap. These maximum enhancements peak at the heavy- and light-hole excitons, showing a key role in the NPoM is the ionization of the bound carriers which can then be extracted.

Further, the stability of the NPoM configuration for solar water splitting was measured in a typical configuration (Figure 4d). The photocurrent decreases by less than 20% over the course of a 1 h experiment. This slow decrease is attributed to the well-documented photocorrosion of the CdSe in solution.²⁸

In conclusion, for the first time, enhanced water-splitting activity on CdSe nanoplatelets placed in plasmonic nanogaps is demonstrated. A 5-fold increase in the photocurrent was measured across a device sparsely covered with AuNPs. The local photocatalytic activity in the plasmonic gaps is estimated to be locally increased by almost 4 orders of magnitude. The use of nanometer-thin semiconductors enables plasmonic coupling throughout the material resulting in dramatically higher electromagnetic field enhancements compared to single nanoparticles. The photocorrosion of CdSe under optical is a problem, limiting its long-term durability. This scheme, however, is not limited to CdSe but can easily be extended to thin films of other photocatalytic materials such as α -Fe₂O₃, Cu₂O, and many others. Further improvement is expected for a closer matching of the catalyst's absorption bands and the plasmon resonance. Nanometer-thick semiconductors overcome the complications incurred from the limited charge-carrier diffusion lengths because all excitons are produced near the surface. Employing ultrathin semiconductor layers reduces the usage of expensive and often toxic materials and can potentially lead to the design of flexible devices, opening entirely new possibilities for solar energy production. Because photons incident on regions outside the plasmonic hotspots are not absorbed, simple corrugation and crumpling of these flexible sheets on plastic substrates can lead to very high total efficiencies.

EXPERIMENTAL METHODS

Sample Preparation. Silicon surfaces were electron-beam evaporated with 70 nm of gold on top of a 5 nm thick chromium adhesion layer. The surfaces were then immersed in 10 mM 4-aminothiophenol (ATP) ethanolic solution for 24 h to ensure monolayer coverage and then rinsed. The samples

were dipped in colloidal solutions of nanoplatelets in hexane for another 24 h, resulting in a monolayer of platelets on the surface with a coverage of ($\sim 70\%$) as revealed by AFM (Figure 1e). Colloidal AuNPs (100 nm, BBI) were then drop-cast on the surface. Nonbound particles were washed away after ~ 5 min, resulting in a sparse NP surface-coverage with a density of $\sim 5 \times 10^5$ particles mm⁻².

CdSe Platelets. Colloidal CdSe nanoplatelets used in these experiments are oleic-acid-capped and have a thickness of 5 atomic layers, or 1.67 nm.²⁹ The lateral dimensions are typically 10 nm \times 25 nm as revealed by TEM and AFM (Figure 1d,e). The platelet absorption edge is at 550 nm as measured by UV-vis spectra (Figure 2c).

Photocurrent Measurements. A xenon light source (Bentham IL 75E) was used with optical power of 200 mW cm⁻². All potentials are reported against the reversible hydrogen electrode (RHE). The electrolyte was aqueous phosphate buffer at pH 7 without any additive. The voltammetry sweep was performed immediately after the sample was immersed into the electrolyte.

Simulations. Simulations were carried out using the boundary-element method.^{30,31} CdSe platelets were modeled as a layer with refractive index taken from the literature ($n = 2.55$) and with a 1 nm layer of oleic acid refractive index ($n = 1.46$) above and underneath to account for the ligands. The layer was sandwiched between a AuNP and a flat Au surface with dielectric function taken from Johnson and Christy.

ASSOCIATED CONTENT

Supporting Information

Contains the calculation of the local photocurrent enhancement generated in the nanogap as well as an SEM micrograph of the sample surface. This material is available free of charge via the Internet at <http://pubs.acs.org>.

AUTHOR INFORMATION

Corresponding Authors

*E-mail: zhanglw@fudan.edu.cn.

*E-mail: jjb12@cam.ac.uk.

Notes

The authors declare no competing financial interest.

ACKNOWLEDGMENTS

This work was supported by the U.K. EPSRC grant EP/G060649/1 and EPSRC grant EP/L027151/1, Defence Science and Technology Laboratory (DSTL), a Marie Curie Intra-European Fellowship (FP7-PEOPLE-2011-IEF 298012 to L.Z.) and ERC grant 320503 LINASS.

REFERENCES

- (1) Abdi, F. F.; Han, L.; Smets, A. H. M.; Zeman, M.; Dam, B.; van de Krol, R. Efficient Solar Water Splitting by Enhanced Charge Separation in a Bismuth Vanadate-Silicon Tandem Photoelectrode. *Nat. Commun.* **2013**, *4*, 2195.
- (2) Hisatomi, T.; Kubota, J.; Domen, K. Recent Advances in Semiconductors for Photocatalytic and Photoelectrochemical Water Splitting. *Chem. Soc. Rev.* **2014**, *43*, 7520–7535.
- (3) Tachibana, Y.; Vayssieres, L.; Durrant, J. R. Artificial Photosynthesis for Solar Water-Splitting. *Nat. Photonics* **2012**, *6*, 515–518.
- (4) Liu, Z.; Hou, W.; Pavaskar, P.; Aykol, M.; Cronin, S. B. Plasmon Resonant Enhancement of Photocatalytic Water Splitting under Visible Illumination. *Nano Lett.* **2011**, *11*, 1111–1116.

- (5) Linic, S.; Christopher, P.; Ingram, D. B. Plasmonic-Metal Nanostructures for Efficient Conversion of Solar to Chemical Energy. *Nat. Mater.* **2011**, *10*, 911–921.
- (6) Lee, J.; Mubeen, S.; Ji, X.; Stucky, G. D.; Moskovits, M. Plasmonic Photoanodes for Solar Water Splitting with Visible Light. *Nano Lett.* **2012**, *12*, 5014–5019.
- (7) Atwater, H. A.; Polman, A. Plasmonics for Improved Photovoltaic Devices. *Nat. Mater.* **2010**, *9*, 205–213.
- (8) Qiu, J.; Zeng, G.; Pavaskar, P.; Li, Z.; Cronin, S. B. Plasmon-Enhanced Water Splitting on TiO₂-Passivated GaP Photocatalysts. *Phys. Chem. Chem. Phys.* **2014**, *16*, 3115–3121.
- (9) Zhang, W.; Saliba, M.; Stranks, S. D.; Sun, Y.; Shi, X.; Wiesner, U.; Snaith, H. J. Enhancement of Perovskite-Based Solar Cells Employing Core-Shell Metal Nanoparticles. *Nano Lett.* **2013**, *13*, 4505–4510.
- (10) Gao, H.; Liu, C.; Jeong, H. E.; Yang, P. Plasmon-Enhanced Photocatalytic Activity of Iron Oxide on Gold Nanopillars. *ACS Nano* **2012**, *6*, 234–240.
- (11) Seo, D.; Park, G.; Song, H. Plasmonic Monitoring of Catalytic Hydrogen Generation by a Single Nanoparticle Probe. *J. Am. Chem. Soc.* **2012**, *134*, 1221–1227.
- (12) Chen, J.; Wu, J. C. S.; Wu, P. C.; Tsai, D. P. Plasmonic Photocatalyst for H₂ Evolution in Photocatalytic Water Splitting. *J. Phys. Chem. C* **2011**, *115*, 210–216.
- (13) Mubeen, S.; Hernandez-Sosa, G.; Moses, D.; Lee, J.; Moskovits, M. Plasmonic Photosensitization of a Wide Band Gap Semiconductor: Converting Plasmons to Charge Carriers. *Nano Lett.* **2011**, *11*, 5548–5552.
- (14) Warren, S. C.; Thimsen, E. Plasmonic Solar Water Splitting. *Energy Environ. Sci.* **2012**, *5*, 5133.
- (15) Thacker, V. V.; Herrmann, L. O.; Sigle, D. O.; Zhang, T.; Liedl, T.; Baumberg, J. J.; Keyser, U. F. DNA Origami Based Assembly of Gold Nanoparticle Dimers for Surface-Enhanced Raman Scattering. *Nat. Commun.* **2014**, *5*, 3448.
- (16) Mertens, J.; Eiden, A. L.; Sigle, D. O.; Huang, F.; Lombardo, A.; Sun, Z.; Sundaram, R. S.; Colli, A.; Tserkezis, C.; Aizpurua, J.; et al. Controlling Subnanometer Gaps in Plasmonic Dimers Using Graphene. *Nano Lett.* **2013**, *13*, 5033–5038.
- (17) Clavero, C. Plasmon-Induced Hot-Electron Generation at Nanoparticle/metal-Oxide Interfaces for Photovoltaic and Photocatalytic Devices. *Nat. Photonics* **2014**, *8*, 95–103.
- (18) Thomann, I.; Pinaud, B. a.; Chen, Z.; Clemens, B. M.; Jaramillo, T. F.; Brongersma, M. L. Plasmon Enhanced Solar-to-Fuel Energy Conversion. *Nano Lett.* **2011**, *11*, 3440–3446.
- (19) Zheng, Z.; Tachikawa, T.; Majima, T. Single-Particle Study of Pt-Modified Au Nanorods for Plasmon-Enhanced Hydrogen Generation in Visible to Near-Infrared Region. *J. Am. Chem. Soc.* **2014**, *136*, 6870–6873.
- (20) Sigle, D. O.; Hugall, J. T.; Ithurria, S.; Dubertret, B.; Baumberg, J. J. Probing Confined Phonon Modes in Individual CdSe Nanoplatelets Using Surface-Enhanced Raman Scattering. *Phys. Rev. Lett.* **2014**, *113*, 087402.
- (21) Ithurria, S.; Tessier, M. D.; Mahler, B.; Lobo, R. P. S. M.; Dubertret, B.; Efros, A. L. Colloidal Nanoplatelets with Two-Dimensional Electronic Structure. *Nat. Mater.* **2011**, *10*, 936–941.
- (22) Sigle, D. O.; Mertens, J.; Herrmann, L. O.; Bowman, R. W.; Dubertret, B.; Shi, Y.; Yang, H. Y.; Tserkezis, C.; Aizpurua, J.; Baumberg, J. J. Monitoring Morphological Changes in 2D Monolayer Semiconductors Using Atom-Thick Plasmonic Nanocavities. *ACS Nano* **2015**, *9*, 825–830.
- (23) Hagfeldt, A.; Lindstr, H.; Lindquist, S. Photoelectrochemical Studies of Colloidal TiO₂ Films: The Effect of Oxygen Studied by Photocurrent Transients. *J. Electroanal. Chem.* **1995**, *381*, 39–46.
- (24) Cowan, A. J.; Barnett, C. J.; Pendlebury, S. R.; Barroso, M.; Sivula, K.; Grätzel, M.; Durrant, J. R.; Klug, D. R. Activation Energies for the Rate-Limiting Step in Water Photooxidation by Nanostructured A-Fe₂O₃ and TiO₂. *J. Am. Chem. Soc.* **2011**, *133*, 10134–10140.
- (25) Zhong, D. K.; Choi, S.; Gamelin, D. R. Near-Complete Suppression of Surface Recombination in Solar Photoelectrolysis by “Co-Pi” Catalyst-Modified W:BiVO₄. *J. Am. Chem. Soc.* **2011**, *133*, 18370–18377.
- (26) Ingram, D. B.; Linic, S. Photoelectrodes: Evidence for Selective Plasmon-Induced Formation. *J. Am. Chem. Soc.* **2011**, *133*, 5202–5205.
- (27) Li, J.; Cushing, S. K.; Zheng, P.; Meng, F.; Chu, D.; Wu, N. Plasmon-Induced Photonic and Energy-Transfer Enhancement of Solar Water Splitting by a Hematite Nanorod Array. *Nat. Commun.* **2013**, *4*, 2651.
- (28) Frese, K. W., Jr. Electrochemical Studies of Photocorrosion of N-CdSe. *Electrochem. Sci. Technol.* **1983**, *130*, 28–33.
- (29) Mahler, B.; Nadal, B.; Bouet, C.; Patriarche, G.; Dubertret, B. Core/shell Colloidal Semiconductor Nanoplatelets. *J. Am. Chem. Soc.* **2012**, *134*, 18591–18598.
- (30) García de Abajo, F.; Aizpurua, J. Numerical Simulation of Electron Energy Loss near Inhomogeneous Dielectrics. *Phys. Rev. B* **1997**, *56*, 15873–15884.
- (31) García de Abajo, F.; Howie, A. Retarded Field Calculation of Electron Energy Loss in Inhomogeneous Dielectrics. *Phys. Rev. B* **2002**, *65*, 115418.